Boundary Element Method (BEM) for Charged Particle Optics

ABSTRACT

Boundary element method is used for the purpose of ray tracing of charged particles. The results presented here are based on a commercially available package; Lorentz, by Integrated Engineering Software; a.k.a. Enginia Research Inc. First, a brief description of different numerical methods is presented, followed by some known theoretical examples. In all cases, excellent agreement between the theoretical results and the numerical ones is observed. Several of the examples deal with the space charge issue. Child's law and Langmuir-Blodgett's are used to verify these results. Also an example, 743 Test, of launching a particle close to a field discontinuity is presented to show the power of BEM method when it comes to dealing with extreme ratios in the dimensionality within a device.

Keywords: Lorentz, Electron gun, Ion beam, Charged particle optics, Ray tracing, Child, Pierce, Langmuir-Blodgett

Boundary Element Method (BEM) for Charged Particle Optics

Ali Asi, Integrated Engineering Software.

ABSTRACT

Boundary element method is used for the purpose of ray tracing of charged particles. The results presented here are based on a commercially available package; **Lorentz**, by Integrated Engineering Software; a.k.a. Enginia Research Inc. First, a brief description of different numerical methods is presented, followed by some known theoretical examples. In all cases, excellent agreement between the theoretical results and the numerical ones is observed. Several of the examples deal with the space charge issue. Child's law and Langmuir-Blodgett's are used to verify these results. Also an example, *743 Test*, of launching a particle close to a field discontinuity is presented to show the power of BEM method when it comes to dealing with extreme ratios in the dimensionality ($>10^6$) within a device.

Keywords: Lorentz, Electron gun, Ion beam, Charged particle optics, Ray tracing, Child, Pierce, Langmuir-Blodgett

NUMERICAL METHODS

Most of the industrial packages are based on one of the three classes of numerical techniques:

1. **FDM** (Finite Difference Method)
2. **FEM** (Finite Element Method)
3. **BEM** (Boundary Element Method)

FDM is based on utilizing a truncated Taylor series expansion in each coordinate direction. Using this expansion, the differential operator is discretized at each point of a rectangular grid covering the entire region of interest. The biggest advantage of this method is its ease of implementation since the differential operators are easily modeled without much preprocessing. Of course, the trade off is paid in less accuracy and speed and poor modeling of the boundaries compared to the other two methods.

FEM uses a variational formulation over a region covered with non-overlapped and non-separated subareas of some prescribed shape, which are termed elements. The variational quantity to be minimized is the total electrostatic or magnetostatic energy stored in a region. Element geometries and unknowns are expressed by polynomials with nodal values as coefficients. Relating these approximations to the operator equation through minimizing the energy functional yields the solution at the nodes. Even though, this method is considered superior to FDM, but still suffers from some drawbacks. Among them are:

- FEM is geared to solve electric and magnetic potentials. Since in direct ray tracing, the knowledge of the values of electric and/or magnetic field is required, these values have to be extracted by applying some kind of numerical derivative operator to the FEM solution. And numerical derivate operators are very sensitive to numerical, truncation and round off, errors.
- In order to limit the number of triangular elements, simulation space has to be truncated somewhere. Even though, many different schemes have been proposed to deal with this issue, nevertheless, dealing with open region problems has always been a concern for FEM methods.
- For problems involving several orders of magnitude of difference between its smallest and largest details ($\sim 10^6$), such as Fowler-Nordheim field emission guns, the FEM triangular elements have to start with extremely small triangles and gradually adapt themselves to much larger triangles. This will increase the number of unknowns substantially.

BEM, on the other hand, solves for the charge distribution on the boundaries of the structure. Knowing these charges, the potential and field can be directly computed everywhere in space. Following are the highlights of this method:

- It is based on an integral formulation, which is numerically a more favorable approach than discretizing a differential operator.
- Elements are one-dimensional entities placed only on the boundaries of the structure. This will reduce the dimensionality of the problem by one, compared to FDM and FEM. It also makes the modeling of the problem easier and more user friendly. The trade off here is that the matrices generated by BEM are usually smaller and denser matrices, while the other two methods tend to generate larger and sparse matrices.
- Dealing with open region problems is inherently easier with BEM, since elements are only placed on the physical boundaries.
- In problems when extreme ratios exist between smallest and largest details of the structure, BEM will be the method of choice. Usually, in these problems the segment with the smallest detail (the tip of a field emission gun) sits at an electrically isolated segment from the body of the structure. Therefore, the element distribution at the tip can be fine-tuned independent of the element distribution everywhere else.
- Finally, since field and potential everywhere in space are being computed from the actual charge distribution on the boundaries, it will result in extremely accurate results when this method is applied to particle ray tracing.

BOUNDARY ELEMENT METHOD

Starting from Laplace's equation:

$$\nabla^2 \Phi = 0 \qquad [1]$$

For two-dimensional case, the following Green's function can be derived:

$$\nabla^2 G = -\delta(\vec{r} - \vec{r}') \qquad [2]$$

$$G(\vec{r}, \vec{r}') = -\frac{1}{2\pi} \ln|\vec{r} - \vec{r}'| \qquad [3]$$

There are three types of boundary conditions that may be encountered:

Dirichlet:
$$\Phi(\vec{r}) = \int_{\partial B} G(\vec{r}, \vec{r}')\sigma(\vec{r}')dr' \qquad [4]$$

Neumann:
$$\Phi'(\vec{r}) = \int_{\partial B} G'(\vec{r}, \vec{r}')\sigma(\vec{r}')dr' + \frac{\sigma(\vec{r})}{2} \qquad [5]$$

Interface:
$$(\varepsilon_1 - \varepsilon_2)\int_{\partial B} G'(\vec{r}, \vec{r}')\sigma(\vec{r}')dr' + (\varepsilon_1 + \varepsilon_2)\frac{\sigma(\vec{r})}{2} = 0 \qquad [6]$$

Knowing the boundary conditions, the objective of the analysis would be computing the σ distribution, such that it will satisfy the three types of boundary conditions. In general we can relate potential Φ to charge density distribution, σ through an integral operator **L**:

$$L\sigma = \Phi \qquad [7]$$

This operator equation can in turn be solved by Galerkin's method of moments [1].

ORBIT EXAMPLES (NO SPACE CHARGE)

743 Test

The 743 Test is one of the most stringent tests that illustrates the strength and accuracy of LORENTZ in calculating the field values as well as particle trajectories (Figure 1). It is highly doubted that any other finite element based package can pass this test as successfully. The test begins with two coplanar semi-infinite plates charged to equal and opposite potentials. A repelled electron is released from one plate (left) at a distance "1" (one) unit of distance from the joint of the plates (zero gap) and should land at a distance of "743" on the other plate (right).

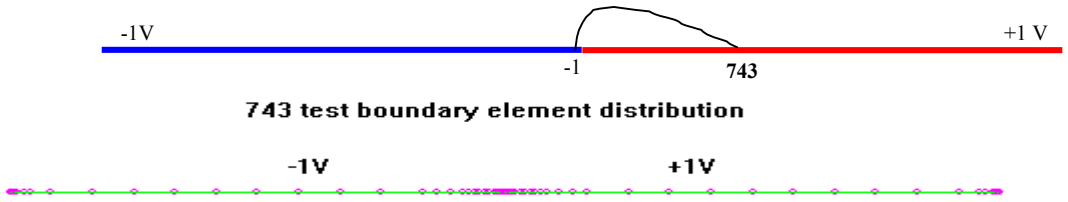

(a)

(b)

Figure 1: (a) The layout of 743 Test (b) The boundary element distribution

In such a structure, the analytic form for the potential is easily obtained by solving the Laplace's equation in polar coordinate system as:

$$\Phi = \frac{2V}{\pi}\tan^{-1}\left(\frac{x}{y}\right) = V\left(1 - \frac{2\theta}{\pi}\right) \qquad [8]$$

where $0 \le \theta = \tan^{-1}\left(\frac{y}{x}\right) \le \pi$ and $V = 1$. From this, the electric field can be obtained using $\vec{E} = -\vec{\nabla}V$ and consequently, the equations of the motion can be solved numerically. This proves "743" as the impact point of the particle with the right

plane. In numerical simulation and also in practice, it is impossible for two segments of different potentials to touch each other. Therefore, during the simulation, a distance of 2×10^{-6} unit length separates the segments. The result of this simulation is presented in Figure 2 and Table 1.

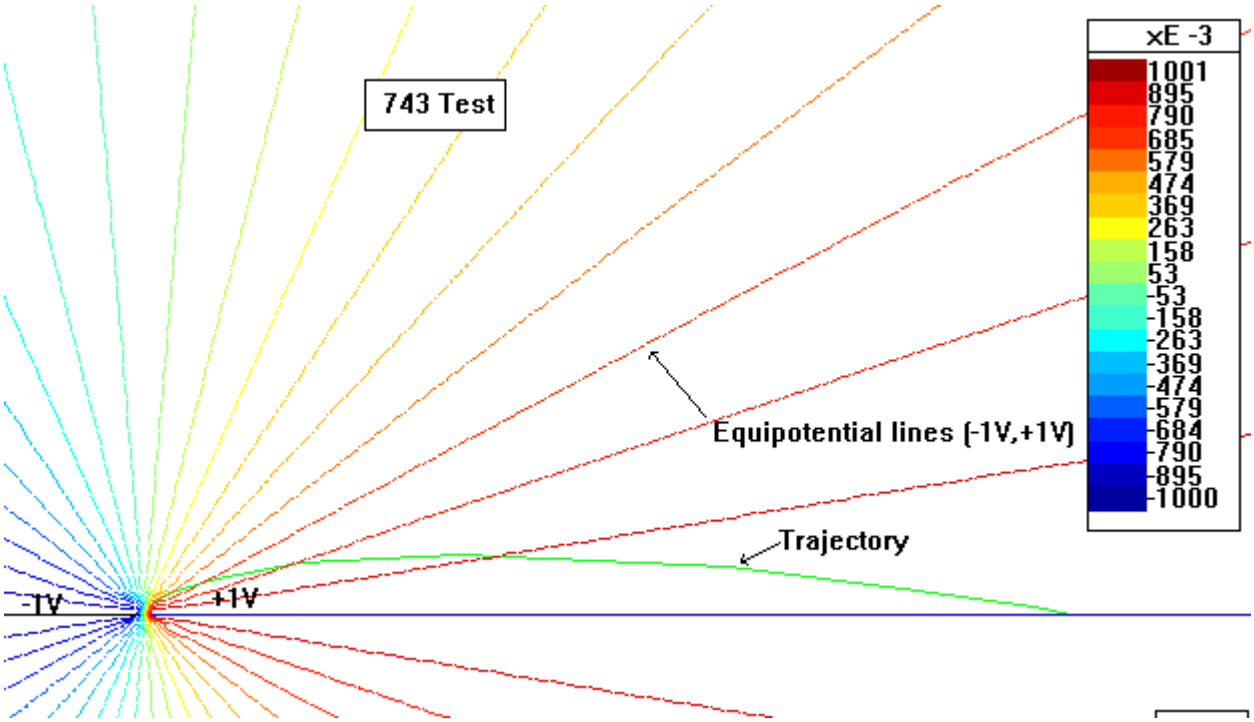

Figure 2: The result of 743 Test simulation depicting both the equipotential lines and the electron trajectory.

	Landing X-coordinate	Error
Lorentz-2D	741	0.27%
Semi-Analytic	743	

Table 1: 743 Test simulation result.

Classical versus relativistic orbits

In this section, several examples of different types of orbits of an electron around a positive nucleus are being presented. Using Gauss's law, the electric field of an infinite cylinder carrying a charge density of ρ_L can be derived as:

$$E_r = \frac{\rho_L}{2\pi\varepsilon_0 r} \quad [9]$$

The following relationship must hold for a circular orbit to exist:

$$eE_r = \frac{mv^2}{r} = \frac{2E_e}{r} \quad [10]$$

In which E_r and E_e are the radial electric field resultant from the nucleus and the electron's energy respectively. By substituting E_r from the first equation into the second one and assuming $\rho_L = 1$:

$$E_e = \frac{\rho_L}{4\pi\varepsilon_0} e = 9\times10^9 e[Joules] = 9[GeV] \quad [11]$$

As shown, the launching energy for establishing a circular orbit around a surface charge of 1 [C/m] is 9 [GeV] and it is independent of the radius of the orbit (circular color trajectory in Figure 3:a). In this example, launching an electron with 9 GeV of energy using Newtonian classical mechanics can only serve an educational purpose. Normally, at these energy levels, Lorentz-2D algorithm switch has to be set to "Einstein" mode (the default). After doing that, another particle with the same 9GeV is launched. Not surprisingly, this second particle did not follow the same circular orbit (moving circle trajectory in Figure 3:a). The reason is simply the fact that our earlier analysis was based on classical mechanics, assuming that the particle mass was an invariant parameter. In order to get back a circular orbit, the analysis has to be revised to account for relativistic effects. For a circular orbit at relativistic speeds, we have:

$$eE = \frac{\gamma m_0 v^2}{r};\ \frac{e\rho_L}{2\pi\varepsilon_0 r} = \frac{\gamma m_0 v^2}{r} \quad [12]$$

in which $\gamma = \frac{1}{\sqrt{1-\beta^2}} = \frac{1}{\sqrt{1-\left(\frac{v}{c}\right)^2}}$, and therefore $v = \beta \cdot c$.

$$\frac{e\rho_L}{2\pi\varepsilon_0} = \frac{m_0\beta^2 c^2}{\sqrt{1-\beta^2}} \quad [13]$$

$$\frac{e\rho_L}{2\pi m_0\varepsilon_0 c^2} = \frac{e\rho_L\mu_0}{2\pi m_0} = \frac{\beta^2}{\sqrt{1-\beta^2}};\ 0 \le \beta < 1 \quad [14]$$

It can be easily shown that for a particle to satisfy this last equation for $\rho_L = 1$, the value of β should be higher than one; i.e. velocities higher than the speed of light, which is impossible. Now, let us assume we want to have a circular orbit for an electron traveling at 90% speed of light; i.e. $\beta = 0.9$. Solving for ρ_L from the last equation results:

$$\rho_L = 52.82768829\frac{\mu C}{m} \quad [15]$$

It has to be pointed out that the reason that the circular orbit is a bit think (Figure 3(b)), is just a display artifact and has nothing to do with the accuracy of the results. Lorentz-2D returns a set of computed points as a result of its ODE solver. In order to give the visual impression of a continuous motion in space, these discrete points are simply connected together using straight lines. Therefore, only the end points of each line segment represent the actual computed points with the accuracy of 1 part per million; i.e. 0.0001%.

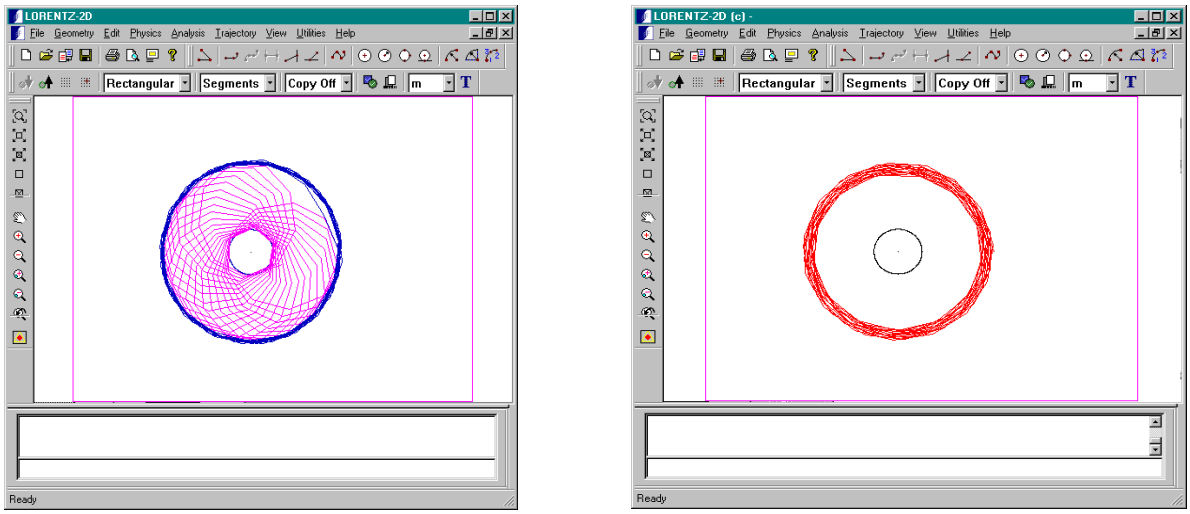

(a) (b)

Figure 3: (a) Circular orbit of a 9 GeV electron around a $1\frac{C}{m}$ nucleus using Classical mechanics and the moving circular orbit of the same particle analyzed using relativistic mechanics. (b) Circular orbit of the same particle can again be achieved by reducing the nucleus charge to $52.82768829\frac{\mu C}{m}$.

Conic sections using Runge-Kutta and Bulirsch-Stoer methods

In this section, the results for some conic section orbits are presented. In order to further test the capabilities of the package, two different types of the adaptive ODE solvers in Lorentz-2D have been used (Figure 4a and b). In these examples, a charge of $0.01^{\mu C}/_{m}$ is setup as the nucleus. To get different conic sections, an electron with constant energy of 8.987713eV is being launched with different distances from the nucleus. The nucleus is located at (0,0) and the particles are launched from (0,5), (0,9), (0,10) to traverse a circular, elliptic and parabolic section, respectively (Figure 4c). In all cases, the error less than 10^{-5} or 0.001% is achieved.

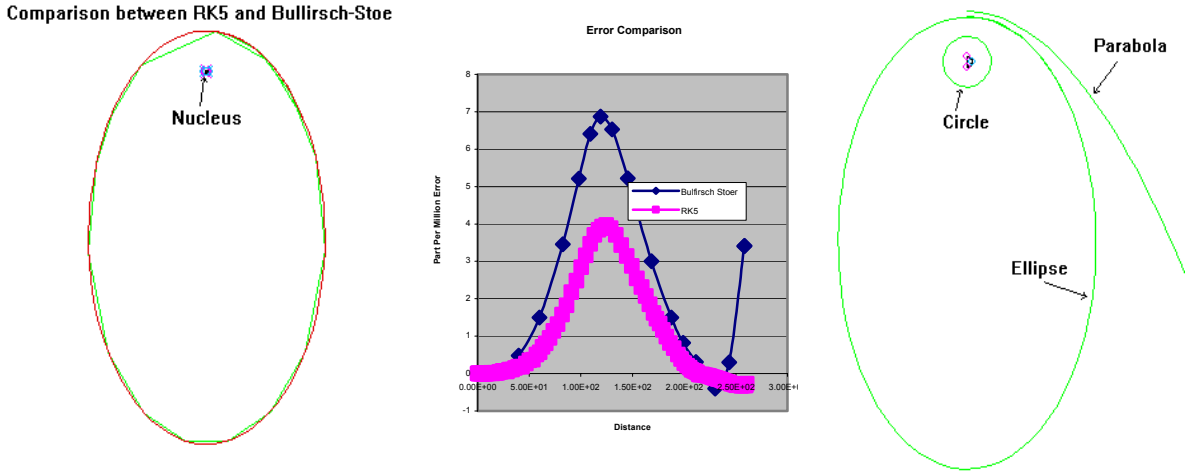

(a) (b) (c)

Figure 4: (a) Comparison of the trajectories of two identical particles analyzed using RK5 (smooth line) and Broken Bulirsch-Stoer method (broken line), (b) Error of RK5 vs. BS (parts per million) (c) Conic sections

CHILD'S LAW

It was Child who first conducted the analysis of a one-dimensional electron flow in saturation regime in 1911. He basically obtained the solution to Poisson's equation:

$$\nabla^2 V = -\frac{\rho}{\varepsilon_0} \qquad [16]$$

Subject to the boundary conditions: $V = 0$ at $z = 0$, $V = V_a$ at $z = d$ and $\frac{dV}{dz} = 0$ at $z = 0$. For the one-dimensional flow in the z-direction, the Poisson's equation can be rewritten as:

$$\frac{d^2 V}{dz^2} = \frac{J}{\varepsilon_0 (2\eta V)^{\frac{1}{2}}}; \ \eta = \frac{e}{m} \qquad [17]$$

with

$$\frac{dV}{dx} = \frac{dV}{dy} = 0 \qquad [18]$$

assumed to be valid everywhere. Under these conditions, Child found the solution to the Poisson's equation to be:

$$V = Az^{\frac{4}{3}} \text{ in which } A = \left[\frac{9J}{4\varepsilon_0 (2\eta)^{\frac{1}{2}}} \right] \qquad [19]$$

Now, let's set up a simple one-dimensional model and observe how well Lorentz-2D results will measure up against Child's law. Mathematically, this one-dimensional problem is equivalent to two infinitely long parallel plates set at voltages 0 and V_a, placed at a distance of d apart. But, numerically, it is not possible to model an infinitely long space. Alternatively, we can model a cylindrical cut of this parallel plate structure, Figure 5(a), and set the surrounding wall as a Neumann boundary condition of $\frac{dV}{dn} = 0$. In Lorentz-2D, this can be achieved by defining a rectangle as illustrated in Figure 5(b), and set the $x = 0$ as the axis of rotation.

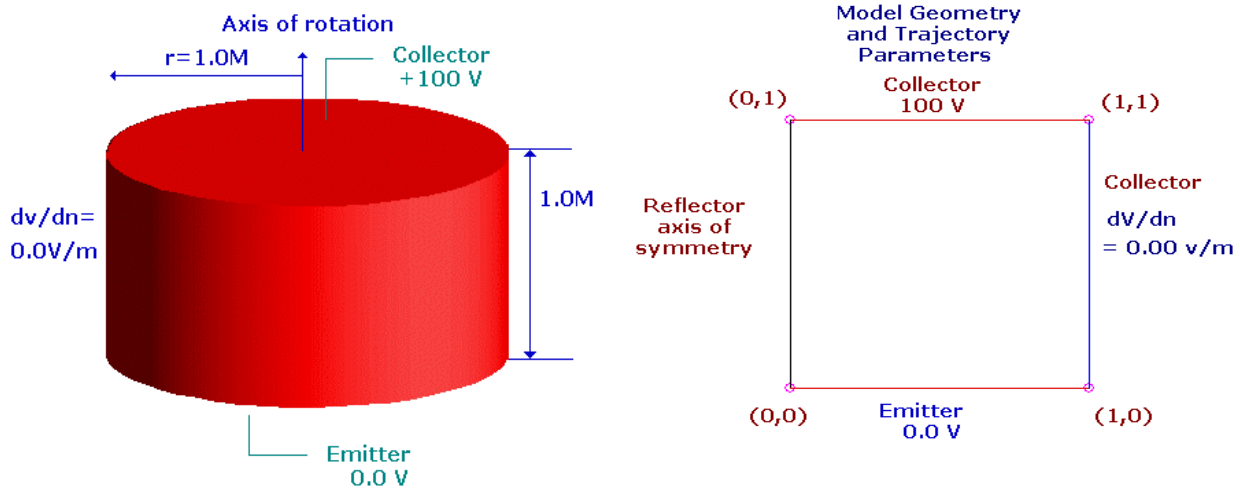

(a) (b)

Figure 5: (a) Solid view of a one-dimensional planar diode. (b) The structure as it is implemented in Lorentz-2D.

Figure 6(a) illustrates the boundary element distribution needed to model this problem accurately. In order to model the space charge effect, a mesh of triangular subareas, Figure 6(b), has to be laid over the region where the particles pass through. Another artificial segment, shadow emitter, is also being introduced. This segment will partition the region into two regions. The smaller region is the one that sits in the close proximity of the emitter and will be treated differently than the other region. This is due to the fact that exactly when the Child's law is being satisfied, i.e. the device is pumped into saturation; the space

charge density right at the neighborhood of the emitter surface goes to infinity. Numerically, this can be achieved by modeling the singular function in that region. The existence of the shadow emitter gives the software the opportunity to deal with this phenomenon.

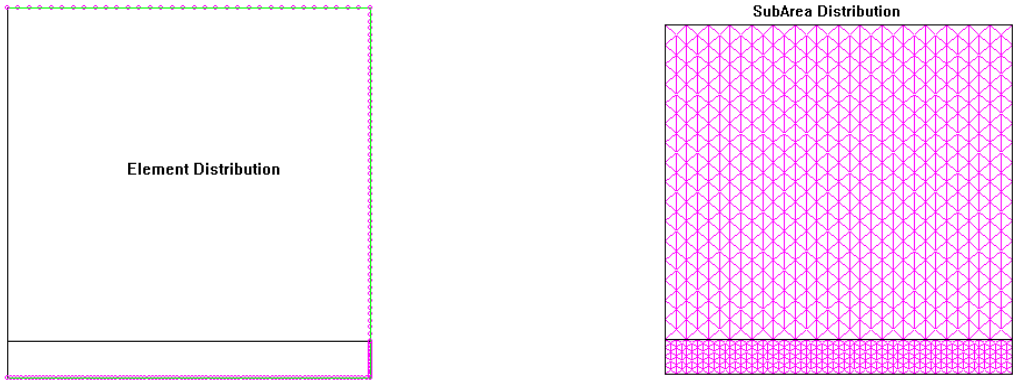

(a) (b)

Figure 6: (a) Boundary element distribution. (b) Sub-area distribution for modeling the space charge

The results of the analysis are summarized in Figure 7 and Table 2, which depicts excellent agreement between computed results and the predictions of Child's law.

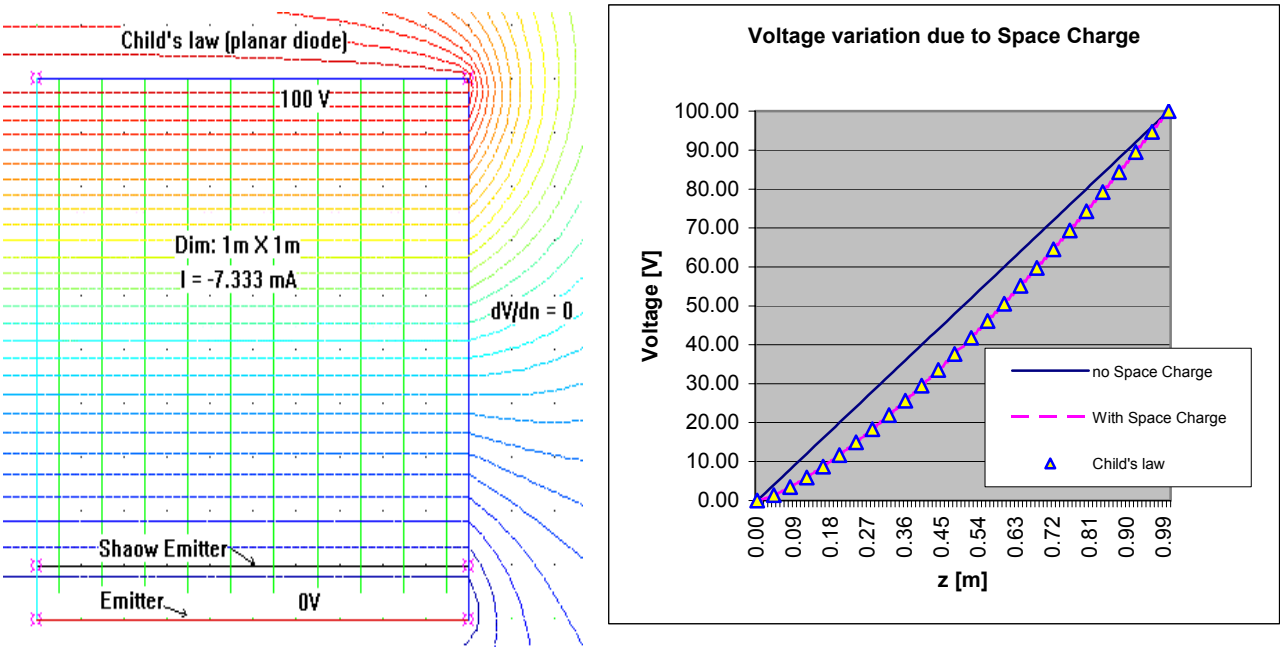

(a) (b)

Figure 7: (a) Voltage contour plot and trajectories (b) Voltage drop along the line [(0.5,0) - (0.5,1)].

	$J\left[\frac{mA}{m^2}\right]$	$I[mA]$	Error
Lorentz (RS)	-2.33	-7.333	0.14%
Theory (RS)	-2.33	-7.322	

Table 2: Planar diode current and current density results.

LANGMUIR-BLODGETT

While Child's law is the basis of many developments that had taken place in electron gun design, it is only applicable to one dimensional planar diode case or the limited area of a problem where it can be approximated as such. Another case, which has received special treatment in the literature, is spherical diode structure, which has been formulated in terms of Langmuir-Blodgett equation. Once again, Lorentz-2D is being used to analyze a spherical diode structure and compare its results with the theoretical predictions.

$$\frac{I}{V^{\frac{3}{2}}} = \frac{16\pi\varepsilon_0\sqrt{2\eta}}{9\alpha^2};\alpha = \gamma - 0.3\gamma^2 + 0.075\gamma^3 - 0.001432\gamma^4 + 0.002161\gamma^5 - 0.00035\gamma^6;\gamma = \ln\left(\frac{r}{r_c}\right) \qquad [20]$$

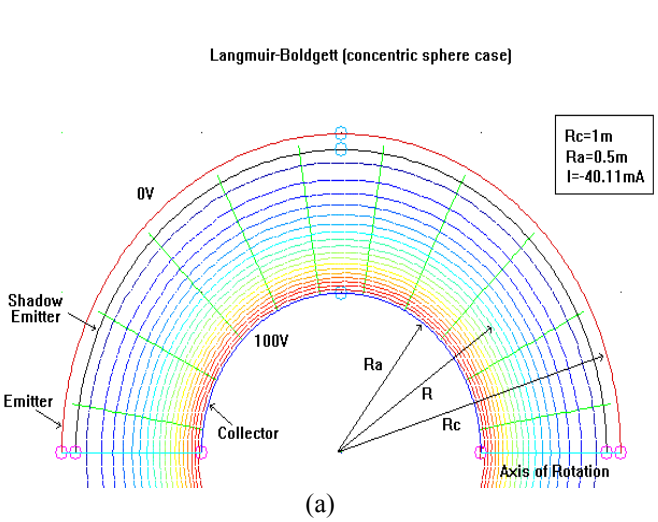

(a)

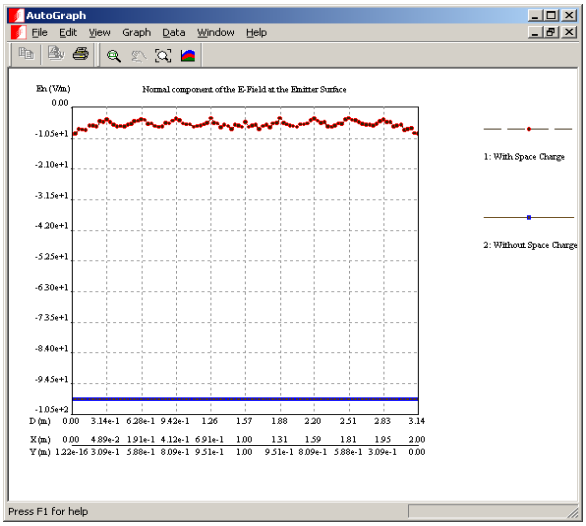

(b)

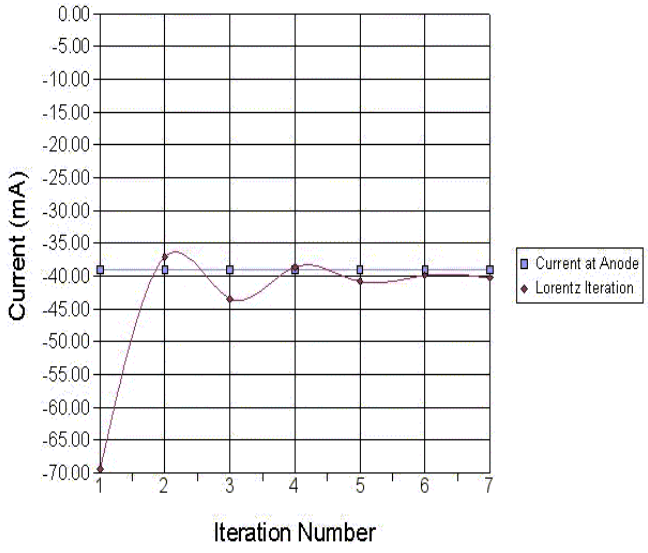

(c)

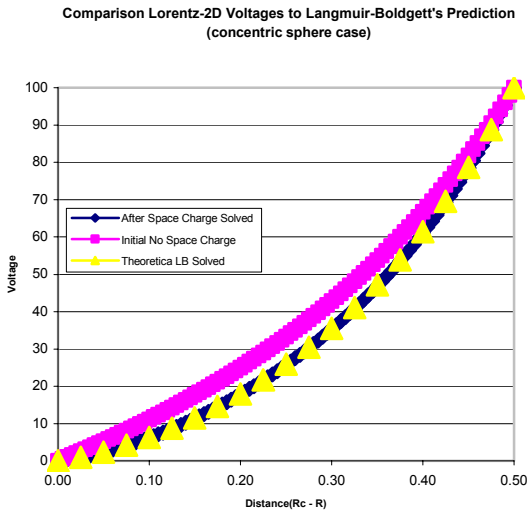

d)

Figure 8: (a) Voltage contour plots and trajectories of a spherical diode (b) Normal component of electric field at the emitter surface with and without the space charge (c) Convergence of the total computed current versus iteration number (d) Voltage drop along a radial line connecting the emitter to the collector.

	$J\left[\frac{mA}{m^2}\right]$	$I[mA]$	Error
Lorentz (RS)	-3.25	-40.11	2.7%
Theory (RS)	-3.11	-39.06	

Table 3: Spherical diode current computation

PIERCE GUN

In this section, the results for a Pierce gun [2] with known theoretical answer are presented. According to Pierce, in order to maintain a parallel flow of electrons, in the presence of space charge, a focusing electrode has to be attached to the emitting surface. The angle between this surface and emitter should be exactly 67.5°.

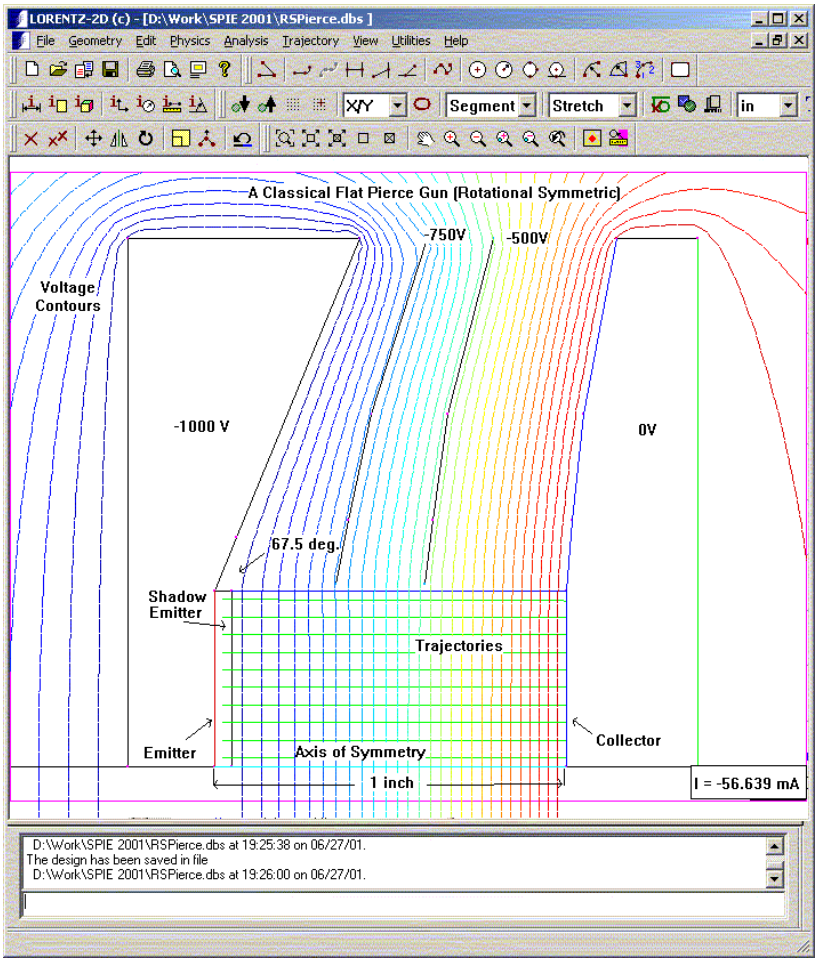

Figure 9: Equipotential lines and trajectories for a classical Pierce Gun

Here, Lorentz-2D is used to model this structure in both two-dimensional (2D) and Rotational Symmetric (RS) case. Again, results from both cases match the theoretical results quite nicely.

	$J\left[\frac{A}{m^2}\right]$	$I\left[\frac{A}{m}\right]$	Error
Lorentz (2D)	-113.37	-1.440	0.76%
Theory (2D)	-114.24	-1.451	

Table 4: Total emitted current (two dimensional Gun)

	$J\left[\frac{A}{m^2}\right]$	$I[mA]$	Error
Lorentz (RS)	-112.52	-56.639	1.5%
Theory (RS)	-114.24	-57.887	

Table 5: Total emitted current (Rotational Symmetric)

Using a built in plotting package, i.e. AutoGraph, the normal component of electric field before and after the space charge computation is plotted. As it is expected, there will be a substantial drop in the normal component of the electric field. Also, noticeable is the fact that the pierce configuration has actually managed to create an almost uniform electric field at the emitter surface. This is expected as Pierce Gun is designed to create a uniform flow of particles.

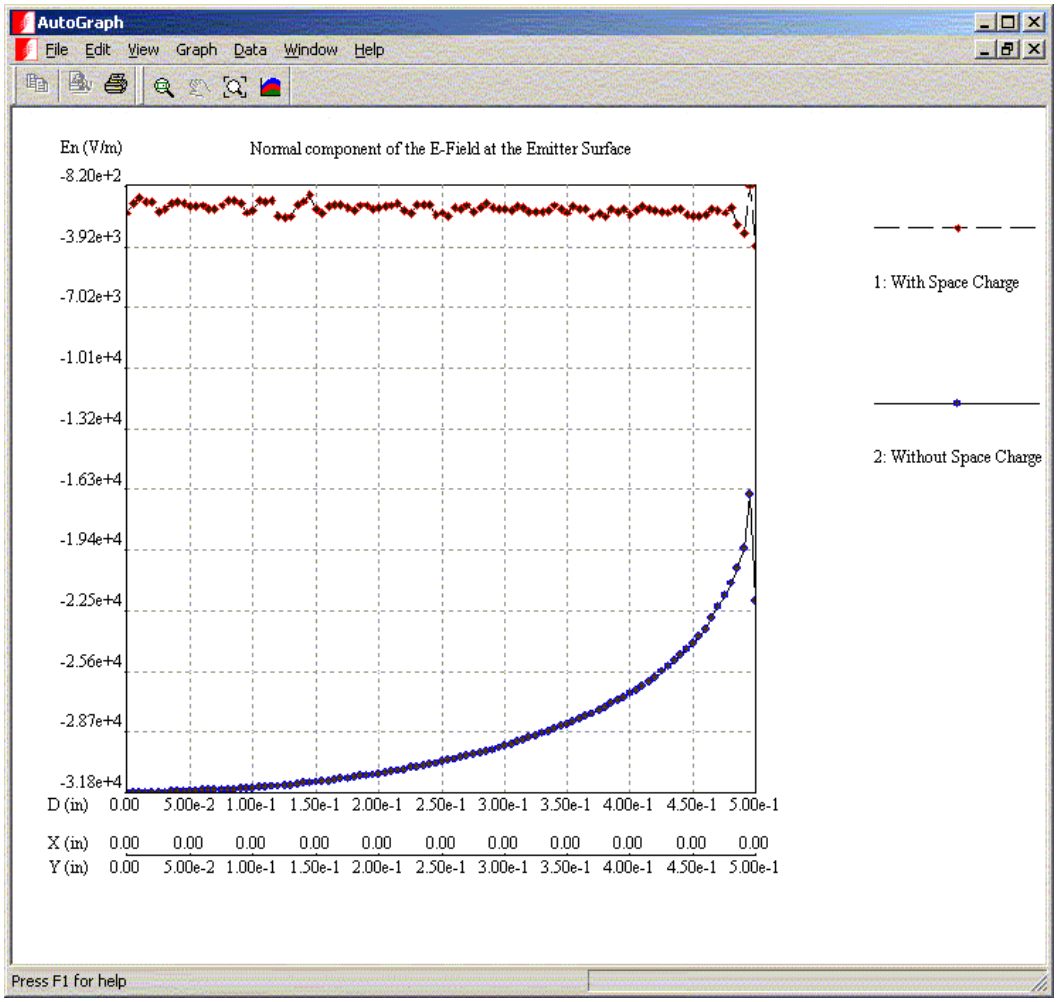

Figure 10: Normal component of the electric field (at the emitter surface) before and after the space charge computation.

ACKNOWLEDGEMENTS

I would like to gratefully acknowledge the help and contributions made by all my colleagues at Enginia Research Inc. without their help this work would have been impossible. Special thanks goes to D. Owsianyk, J. Dietrich, and G. Bilbrough for helping me compile some of the data presented. I am also indebted to Mr. Bob Klinkowstein from Newton Scientific Inc. for devising the Pierce Gun test.

REFERENCES

1. Y. B. Yildir, K.M. Prasad, D. Zheng, "Computer Aided Design in Electromagnetic Systems: Boundary Element Method and Applications," Control and Dynamics Systems, vol. 59, pp. 167-223, 1993.
2. A. Septier, Focusing of Charged Particles, Vol. II, pp. 29-35, Academic Press, Inc., 1967.

asi@enginia.com;
Phone: (204) 632-5636; fax: (204) 633-7780;
http://www.integratedsoft.com;
R&D Department,
Integrated Engineering Software,
300 Cree Crescent,
Winnipeg, Manitoba,
Canada R3J-3W9.